

Automated Optic Nerve Disc Parameterization

Povilas TREIGYS, Vydūnas ŠALTENIS, Gintautas DZEMYDA

*Department of System Analysis, Institute of Mathematics and Informatics
Akademijos 4, LT-08663 Vilnius, Lithuania
e-mail: treigys@ktl.mii.lt, dzemyda@ktl.mii.lt*

Valerijus BARZDŽIUKAS, Alvydas PAUNKSNIS

*Department of Ophthalmology, Institute for Biomedical Research, Kaunas University of Medicine
Eiveniu 4, LT-3007 Kaunas, Lithuania
e-mail: vb@tmc.kmu.lt, apaun@medi.lt*

Received: 2 January 2008; accepted: 6 June 2008

Abstract. New information technologies provide a possibility of collecting a large amount of fundus images into databases. It allows us to use automated processing and classification of images for clinical decisions. Automated localization and parameterization of the optic nerve disc is particularly important in making a diagnosis of glaucoma, because the main symptoms in these cases are relations between the optic nerve and cupping parameters. This article describes the automated algorithm for the optic nerve disc localization and parameterization by an ellipse within colour retinal images. The testing results are discussed as well.

Keywords: optic nerve disc, optic nerve head, optic nerve excavation neuroretinal rim, automated localization, parameterization.

1. Introduction

Eye fundus examination is one of the most important diagnostic procedures in ophthalmology. A high quality colour photograph of the eye fundus is helpful in the accommodation and follow-up of the development of the eye disease. Evaluation of the eye fundus images is complicated because of the variety of anatomical structure and possible fundus changes in eye diseases. Sometimes it requires high-skilled experts for evaluation.

The ways of a better fundus image evaluation is the use of modern information technologies for processing and parameterization of the main structures of the eye fundus.

There are three main structures in the eye fundus image, used for making a diagnosis in ophthalmology:

- 1) optic nerve disc;
- 2) blood vessels (retinal arteries and veins);
- 3) retina.

The optic nerve disc is the main structure for localizing other eye fundus structures as well as a very important structure for diagnosing some eye and neurological diseases.

Characterization of such cases is the object of image analysis.

The optic nerve head appears in the normal eye fundus image as a yellowish disc with whitish central cupping (excavation) through which the central retinal artery and vein pass.

Changes of the optic nerve disc can be associated with numerous vision threatening diseases such as glaucoma, optic neuropathy, swelling of the optic nerve head, or related to some systemic disease.

This paper focuses on automated optic nerve disc (OD) localization and approximation by an ellipse in retinal images to produce the parametric form of the optical nerve disc. The intensity of the optic nerve disc is much higher than the surrounding retinal background. Thus the position of OD can roughly be estimated by finding the region or point with the maximum variance (Sinthanayothin *et al.*, 1999). However, such a straightforward method often fails due to non-uniform illumination or photographic noise seen in the retinal images.

The first problem of automated OD localization is to identify its position in retinal images. In the literature, there are many algorithms for OD localization. Basically these methods deal with image segmentation, dynamic contours and geometric models.

In (Sinthanayothin *et al.*, 1999; Boyd, 1996) the vessel detection and convergence analysis are based on the region of nearly vertical vessels emanating in the area of OD. This algorithm led the authors to achieve an accuracy of 80%. A separate case of convergence analysis is introduced in (Hoover and Goldbaum, 2003). Here every vessel forms a separate line and the voting for the constructed lines is performed. Since this is an extension of methods (Boyd, 1996; Chaudhuri *et al.*, 1989) this provides the accuracy of 89%. In the paper (Tobin *et al.*, 2006) is described an accurate vasculature segmentation method and achieve the localization accuracy up to 87%. Also segmentation method is presented in paper (Grau *et al.*, 2006). In this paper authors discusses anisotropic Markov random field models for gathering prior knowledge of the geometry of the optic nerve disc structure. A different approach was used in (Goldbaum *et al.*, 1996), where the main idea is segmentation accomplished by using matched spatial filters of bright and dark blobs. However, quantitative results for nerve localization were not provided. In (Pinz *et al.*, 1998) the localization of optical nerve disc is accomplished by segmenting a retinal image into vessels, fovea, and nerve. The lack of this method is that the authors have a priori knowledge where OD is in the retinal image, and the data set used was very small. The accuracy of this method is 91%. Segmentation and the vessel tracking methods are also presented in (Tolias and Panas, 1998). Nerve localization is based on the brightest region search in a restricted third of the image. The testing data set consisted only of three fundus images, so the results are very questionable. The use of active dynamic contours, described in (Morris and Donnison, 1999), is introduced, too. The main idea is that edge gradients and terminations in the image are converted into energies. This covers the actual OD by a curve. This approach is explored in article (Xu *et al.*, 2007). In this article authors presents modified active contour algorithm by introducing knowledge-based clustering and smoothing update techniques. This allows authors to achieve better success rate (94%) compared to standard gradient vector flow snake model (12%). Geometric models, presented in (Foracchia *et al.*, 2004), probe the fundus image in a spatial

or frequency domain with a predefined model for optic nerve disc localization. Another approach is presented in (Lowell *et al.*, 2004). Here authors deals with blurred images from diabetic screening programme. Article incorporates specialized template matching filters and active segmentation methods for OD localization and leads to accuracy of edge Excellent-fair performance (evaluated by ophthalmologist) of 83%.

Almost all of these methods rely on the quality of vasculature segmentation.

The automated optic nerve disc approximation by a parametric curve such as an ellipse is a second goal of this paper. Of course, 3D model parameters of optic disc could be much more informative, but this is not possible to explore, since this problem is related to the equipment involved with 3D photography.

However, the OD parameterization is insufficiently explored. The research is mostly concentrated on exudates, drusen detection and parameterization, but not the optical disc itself.

This problem is extremely difficult since, in general, the OD in the retinal image does not have a homogenous structure. This is due to a vascular tree within the optic nerve disc, and we have to deal with colour images. This article describes an algorithm for OD localization in retinal images and parameterization by an ellipse.

Use of new information technologies provides a possibility of collecting a large amount of fundus images into databases. It allows us to use automated processing and classification of images for clinical decisions.

The automated localization and parameterization of the optic nerve head is particularly important in making a diagnosis of glaucoma, because the main symptoms in these cases are links between the optic nerve and cupping parameters and differences in the symmetry between eyes. Besides, tracking of the disease progress is almost impossible without a quantitative change in patient's fundus images with the lapse of time. Thus, the parameterization of the optic nerve disc is crucial.

2. Image Pre-Processing and Scaling

The eye fundus images were collected in the Department of Ophthalmology of the Institute for Biomedical Research of Kaunas University of Medicine, using the fundus camera *Canon CF-60UVi*, at a 60° angle. 6,3 Mpixel images (image size 3072×2048 pixels) were taken. The magnification quotient was 0,0065248 mm/pixels, common magnification quotient for the system eye-fundus camera was $0,556782 \pm 0,000827$ (mean \pm SD). The scale (mm/pixels) for the fundus camera was 0,01171875 mm/pixels.

In order to localize OD, first of all we have to pre-process an image. The first step of image pre-processing is accomplished by scaling down the retinal image to the size of 768×512 pixels. Scaling is performed in order to decrease the computation time. Basically the circular *Hough* transform is the most time consuming procedure, since for every pixel in a spatial domain it calculates circle of radius r in a *Hough* space. In the case of the initial image, it has to be done 6291456 times. In the case of a scaled down image it has to be done 16 times less. This leads to a substantial acceleration of approximation

by the ellipse, which is very important at this stage. Besides, the size of the optic nerve disc is much larger than the details lost in the scaling operation. Also, as shown in the results section, quantitative parameters have a minor difference between that, achieved from a non-scaled image, and those achieved from the scaled down fundus image.

Since the blood vessels are located within the area of the optic nerve disc and we will search for a round object in the image, the second step of pre-processing is to remove the vessels from the area of OD. Segmentation methods work on a gradient image and lock onto homogeneous regions enclosed by strong gradient information. This task is extremely difficult in our context since the optic disc region, as mentioned before, is invariably fragmented into multiple regions by the blood vessels.

2.1. Mathematical Morphology

Morphological operations typically probe an image with a small shape or template known as a structuring element. The four basic morphological operations are erosion, dilation, opening, and closing (Soille, 1999). The grey-scale erosion can be described as a calculation of the minimum pixel value within the structuring element centred on the current pixel $A_{i,j}$. Denoting an image by I and a structuring element by Z , the *erosion* operation $I \ominus Z$ at a particular pixel (x, y) is defined as

$$I \ominus Z = \min_{(i,j) \in Z} (A_{x+i,y+j}), \quad (1)$$

where i and j index the pixels of Z .

The grey-scale *dilation* is considered in a dual manner and thus can be written as

$$I \oplus Z = \max_{(i,j) \in Z} (A_{x+i,y+j}). \quad (2)$$

The *opening* of an image is defined as erosion followed by dilation, while the image closing includes dilation followed by erosion. Thus, the morphological operation as *closing* can be defined as follows:

$$I \bullet Z = (I \oplus Z) \ominus Z = \min_{(i,j) \in Z} \left(\max_{(i,j) \in Z} (A_{x+i,y+j}) \right). \quad (3)$$

The closing operator usually smoothes away the small-scale dark structures from colour retinal images. As closing only eliminates the image details smaller than the structuring element used, it is convenient to set the structuring element big enough to cover all possible vascular structures, but still small enough to keep the actual edge of the OD. Mendels *et al.* (1999) applied the closing grey-level morphology operation to smooth the vascular structures while keeping the actual edges of the optic disc.

The fundamental concepts of grey-level morphology operations cannot be directly applied to colour images (Goutsias *et al.*, 1995). Each colour retinal image I can be described as a set of three independent vectors $\{R, G, B\}$. If we assume that each of these vectors represents a grey-scale image (Fig. 1), we can apply the morphological closing

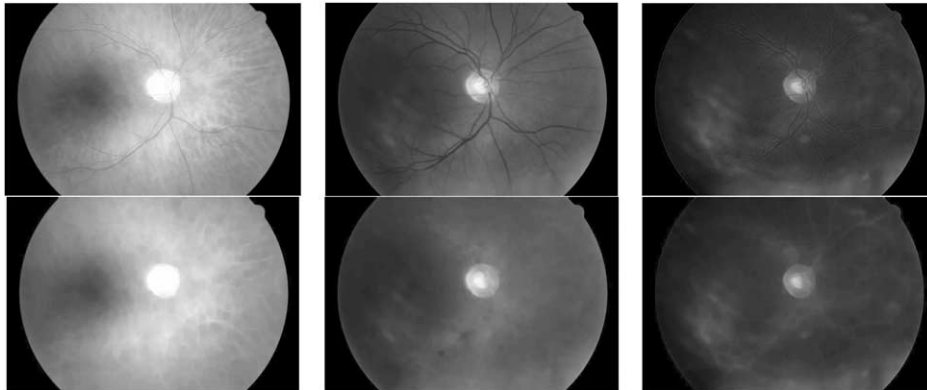


Fig. 1. The top row is a colour image decomposed into colour vectors; the bottom row shows images after morphological closing.

operation (3) to each colour vector with the disc structuring element whose diameter is 14 pixels. The diameter of the structuring element should not be smaller than the widest vessel underlying in the image. Thus, in our case, the vessels are not wider than 14 pixels.

2.2. Recombination of the Results

After decomposing the retinal image into R , G , and B bands and processing each band separately, we can recombine the results. However, a recombined result is not valid in general.

As described by Peters (1997), let us consider a separate erosion of R , G , and B bands, using the structuring element Z . Each pixel after erosion ($R \ominus Z$) is the minimum value of initial R within the structuring element neighbourhood of the pixel. Descriptions of $G \ominus Z$, $B \ominus Z$ are similar. The problem is that the minimum is valid only for the separate R , G , B bands. After we recombine those separate bands into the structure for colour representation, it becomes not clear which minimum to use. Thus, this violates the property of erosion (1) where the minimum has to be over all the three bands within the structuring element Z . The same scheme results in dilation.

However, the recombination of processed bands of the retinal image does not introduce a colour distortion and we achieve a *closed* colour retinal image (Fig. 2). The colour distortion is avoided because, in general, the morphological closing fills the dark holes in bright regions. Further, the optic nerve disc is a bright region in the retinal image, and the brighter the region, the higher the value of each band's pixel brightness. Hence, by selecting an appropriate structuring element's size, we eliminate dark regions formed by vasculature and replace them by the surrounding brighter region, located around the vessels replaced.

In further investigation, in order not to lose the optic disc details, we will use the *closed* colour retinal image converted to grey-scale, since the OD edge describes all the three colour bands. This approach suffers from unwanted details seen in the R and B

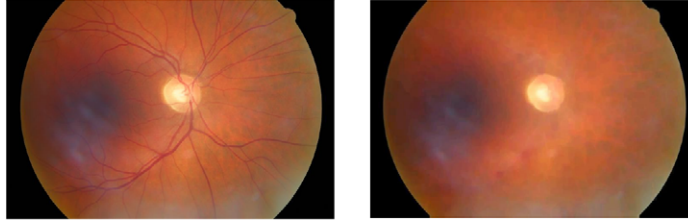


Fig. 2. The initial retinal image is shown on the left; the *closed* colour image is shown on the right.

bands, which do not belong to the optic nerve disc. Thus, as a reference the closed G band fundus image for the same patient's eye is also used which is least polluted with additional details.

3. Localization of the Optical Nerve Disc

After the pre-processing step has been completed, we have to localize the OD center. The difficulty is that we even do not know a priori where the optical disc lies in the retinal image. Thus, localization is performed in two steps, by applying the *Canny* edge detector and *Hough* transform to the edge-detected image.

3.1. Edge Detection

The *Canny* operator is one of the most widely used edge detection algorithms due to its performance. *Canny* has defined three criteria to derive the equation of an optimal filter for step edge detection: *good detection*, *good localization*, and clear response (only one response to the edge) (Canny, 1986). We describe a scheme of the *Canny* edge detector algorithm.

The first step is to filter out any noise in the original image before trying to detect and locate any edges. Consider a two-dimensional *Gaussian* function:

$$G_{\sigma} = \frac{1}{\sqrt{2\pi\sigma^2}} e^{-\frac{i^2+j^2}{2\sigma^2}}, \quad i = 1 \dots n, \quad j = 1 \dots m. \quad (4)$$

The main advantage of the *Gaussian* function is that we can easily approximate by a discrete convolution kernel. The discrete approximation can be calculated using

$$h_g(i, j) = e^{-\frac{i^2+j^2}{2\sigma^2}}, \quad (5)$$

$$h(i, j) = \frac{h_g(i, j)}{\sum_i \sum_j h_g}, \quad (6)$$

where m, n are the dimensions of the discrete approximation matrix. In our case, the standard deviation for noise suppression used $\sigma = 2$. This parameter is set experimentally.

Once a suitable mask has been calculated, the *Gaussian* smoothing is performed using the standard convolution methods.

3.2. Edge Gradient Detection

After smoothing the image and eliminating the noise, the next step is to find the edge strength by taking the gradient of the image.

Thus, for each pixel value at (x, y) in the smoothed retinal image I , we calculate

$$\nabla I(x, y) = (I_x(x, y), I_y(x, y))', \quad (7)$$

where $I_x(x, y)$, $I_y(x, y)$ are image gradients along the x and y axis, respectively.

Calculation of edge strength is performed by

$$E_s(x, y) = \sqrt{I_x^2(x, y) + I_y^2(x, y)}. \quad (8)$$

Once the gradient has been found, the calculation of its direction comes to be possible:

$$E_o(x, y) = \arctan\left(\frac{I_x(x, y)}{I_y(x, y)}\right). \quad (9)$$

Further non-maximum suppression has to be applied. There are only four directions when describing the surrounding pixel degrees: 0, 45, 90, and 135. Thus, each pixel has to be grouped in one of these directions to which it is closest. Next we check whether each non-zero pixel (x, y) in the image is greater than its two neighbours perpendicular to the gradient direction $E_o(x, y)$. If so, keep the pixel (x, y) , or else set it to 0.

And the final phase of the *Canny* edge detector is to apply the hysteresis threshold.

3.2.1. Otsu's Threshold Method

By thresholding the previous result at two different levels τ_1 and τ_2 , we obtain two binary images T_1 and T_2 . The difficulty is that we cannot apply the static threshold level τ_1 since there are no retinal images with identical properties. For automated threshold level calculation we use *Otsu's* method (Otsu, 1979).

Otsu's method maximizes the a posteriori between-class variance $\sigma_B^2(t)$ given by

$$\sigma_B^2(t) = w_0(\tau_1)[1 - w_0(\tau_1)] \left(\frac{\mu_T(\tau_1) - \mu_1(\tau_1)}{1 - w_0(\tau_1)} - \frac{\mu_1(\tau_1)}{w_0(\tau_1)} \right), \quad (10)$$

where

$$w_0(\tau_1) = \sum_{i=0}^{\tau_1} \frac{n_i}{N}; \quad w_1(\tau_1) = 1 - w_0(\tau_1);$$

$$\mu_1(\tau_1) = \sum_{i=0}^{\tau_1} i \frac{n_i}{N}; \quad \mu_T(\tau_1) = \sum_{i=0}^{L-1} i \frac{n_i}{N}.$$

The optimal threshold τ_1 is found by *Otsu's* method through a sequential search for the maximum of $\max_{0 \leq \tau_1 < L} \sigma_B^2(\tau_1)$ of τ_1 , where n_i represents the number of pixels in

the grey-level i , L is the number of grey-levels, and N is the total number of pixels in the image (Tian *et al.*, 2003).

We assume that to calculate the threshold level τ_1 , the black background around the retina is omitted. Also, after image pre-processing, a supplementary noise is observed. This leads to the appearance of unwanted details since, in origin, *Otus's* method was designed for weak gradient change detection. After the threshold, described in the next section, the edge detected images contain too many edge details. Thus, after a careful computation, the original parameter τ_1 is scaled to 25% and the parameter τ_2 is calculated as follows: $\tau_2 = 0.1\tau_1$.

3.2.2. Hysteresis Threshold

After the parameters τ_1 and τ_2 have been calculated, we threshold the image at these two levels. For all unvisited pixels (x, y) in the image T_2 we trace each segment in T_2 to its end and set them as contour points. At the segment end in the image T_2 we seek its neighbours in the image T_1 (since this image has much more details). If there are neighbouring pixels in the image T_1 , we denote them as contour points, too.

As described in the recombination of the results section, to detect edges, we use grey-level images from the *closed* band G , and the *closed* colour retinal image converted to grey-scale. This is necessary because there are cases where band G does not provide any information about OD, and the bands B , R are very noisy. In addition, using the *closed* grey-scale image with all bands, we retain all the nested information about OD.

The results of the edge detection scheme described are shown in Figs. 3, 4.

Here, in the right-side figures, the boundaries of OD are displayed 5 times magnified.

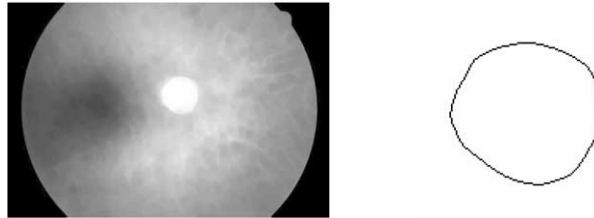


Fig. 3. The closed G band image after edge detection.

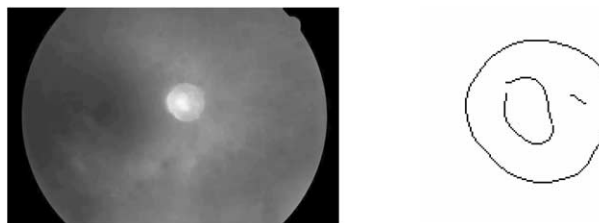


Fig. 4. The *closed* grey-level retinal image after edge detection.

3.3. Applying Hough Transform in the Optic Nerve Disc Localization

After the edge detection has been completed, we apply the *Hough* transform (Hough, 1965) to the optic nerve disc localization. This is necessary because the optic disc structure in retinal images is nearly circular. We describe here the main idea. The general *Hough* transform can be found in (Ballard, 1981).

The circular *Hough* transform is the method for transforming the image plane into the *Hough* plane. Each picture element in the image plane is transformed into a circle in the *Hough* plane.

Thus, in the case of a circle, this model has three parameters: two parameters indicate the centre of the circle and one parameter the radius. In this scheme the parameter space is congruent with the image space, that is, each point in the image maps to a point in the same position in the parameter space (Ashbrook and Thacker, 1998). To detect a circle of radius r , the circles of this radius are plotted in the *Hough* parameter space centred on every edge pixel found in the image. Thus, an array of peaks is formed for each edge-detected fundus image. A peak emerges when the circles in the *Hough* space intersect one another. Such peaks in the *Hough* parameter space indicate the possible centres of r radius circles.

The problem is that we do not know both: where the OD lies in the retinal image and how large it is. We iterate the circular *Hough* transform each time with the different circle radius r and select the highest peak value in the peak array formed (Fig. 5).

After the parameters for the circle have been selected, we assume that we have approximately found the OD centre coordinates and optic nerve disc radius. Fig. 6 shows the optic nerve disc boundary after *Canny* edge detection and the resulting iterative *Hough* transform circle (dashed line).

4. Optic Nerve Disc Approximation by the Ellipse

After we have approximately calculated a radius of the circle and its centre coordinates, the next step is to choose the points describing the OD boundary.

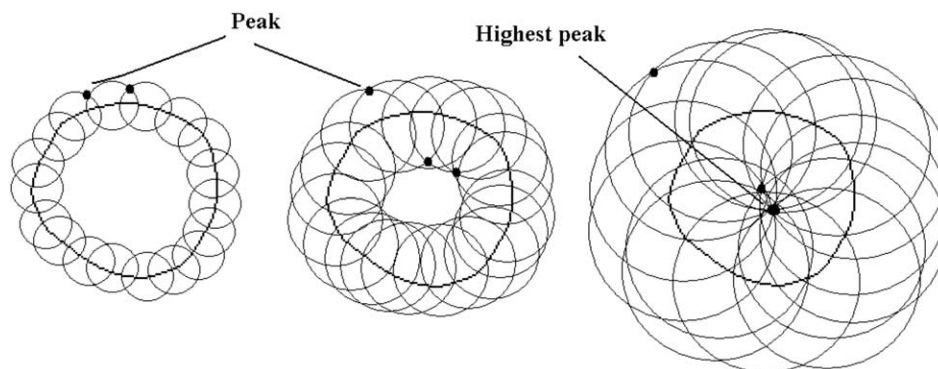


Fig. 5. The location of a circle in the image space is indicated by a highest peak in the peak array.

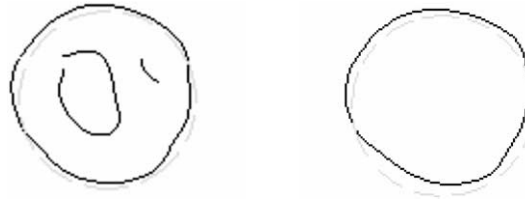


Fig. 6. The result of *Iterative Hough* transform referring to the edge from the retinal image area.

This is done by varying the circle radius on polar coordinates. The OD boundary can lie (as seen in Fig. 6) either within the circle found or outside it. In this case, we state that the binary image point (x, y) is selected as a boundary of the optic disc by iteration

```

phi=0
Do While phi < 2 * pi
  Increase phi
  radius = r*0.9
  Do While (radius < r * 1.1)
    x = Hough centre x + (radius * Cos(phi))
    y = Hough centre y + (radius * Sin(phi))
    If point(x,y)=TRUE Then
      Add point(x,y) to boundary point accumulator
    End If
    Increase radius
  Loop radius
  Increase dphi
Loop phi

```

Here: phi is a direction; $dphi$ is a direction angle step; $radius$ is the current radius, r is the radius obtained by the iterative *Hough* transform.

In other words, we iterate the angle and the radius in polar coordinates, found by the iterative *Hough* transform, and check whether the image point (x, y) is set to 1. If so, we add it to the boundary point accumulator, or else move further to check another point (x, y) .

Here the radius r is restricted to the interval $[r * 0.9, r * 1.1]$, whereas there are many cases where, after detecting the edge inside the area of OD, we see the edges of excavation. As usual, these edges (we assume them to be noise) are located near the OD boundary and can be defined as false ones. Also, the optic disc boundary is not always round or ellipse-shaped after edge detection. Consequently, several fragments of boundary arcs can form a round-shaped structure and other fragments, starting from the true OD boundary, can stretch along the retina as a line (Fig. 7). These lines are no more than noise left from vessel tree removal.

After the optical disc boundary coordinates have been accumulated from both binary images (as described before, from the *closed* grey-level and the *closed* G band image) of



Fig. 7. OD boundaries with noise after edge detection.

the same patient of the same eye, we apply the least squares ellipse fitting algorithm to the parametric form of cone calculation depending on the data set collected.

4.1. Least Squares Method

Since our objective is to parameterize the optic disc by an ellipse, we further introduce the least squares algorithm for fitting the ellipse. A full description of the algorithm can be found in (Fitzgibbon *et al.*, 1999). Since this algorithm solves the best fit problem to the data set, it also controls the rotation of a cone and guarantee that the calculated parameters of an elliptic cone fit best to the given data set.

In general, the cone can be expressed as

$$F(E_{param}, x) = E_{param} \cdot x = ax^2 + bxy + cy^2 + dx + ex + f = 0, \quad (11)$$

where $E_{param} = [a \ b \ c \ d \ e \ f]$ are the parameters of a cone and $x = [x^2 \ xy \ y^2 \ x \ y \ 1]$ are pixel coordinates from the boundary accumulator array. $F(E; x_i)$ is the so-called algebraic distance from the point (x, y) to the cone $F(E_{param}; x) = 0$. So the fitting of the general cone can be approached by minimizing the sum of squared algebraic distances:

$$\Theta_A(E_{param}) = \sum_{i=1}^N F(x_i)^2. \quad (12)$$

Bookstein (1979) has shown that problem (12) can be solved as a problem of eigenvalues

$$D^T D E_{param} = \lambda C E_{param}. \quad (13)$$

Here D is the design matrix and $D = [x_1 \ x_2 \ \dots \ x_n]^T$, C is the constraint matrix.

The appropriate constraint on the ellipse is well known, namely, that the discriminant $b^2 - 4ac$ has to be negative. However, this constrained problem is difficult to solve in general, since the Kuhn–Tucker (Rao, 1984) conditions do not guarantee the solution.

Data scaling is performed by applying $E_{param}^T C E_{param} = 1$ quadratic constraint C of the form

$$E_{param}^T \begin{bmatrix} 0 & 0 & 2 & 0 & 0 & 0 \\ 0 & -1 & 0 & 0 & 0 & 0 \\ 2 & 0 & 0 & 0 & 0 & 0 \\ 0 & 0 & 0 & 0 & 0 & 0 \\ 0 & 0 & 0 & 0 & 0 & 0 \\ 0 & 0 & 0 & 0 & 0 & 0 \end{bmatrix} E_{param} = 1, \quad (14)$$

which compels the constraint to become $4ac - b^2 = 1$. Thus, this reduces the ellipse fitting algorithm to minimizing

$$E = \|D E_{param}\|^2, \quad (15)$$

with respect to the constraint $E_{param}^T C E_{param} = 1$.

Therefore, by differentiating the equation and assuming that λ is a *Lagrange* multiplier, we arrive at the system of equations:

$$S E_{param} = \lambda C E_{param}, \quad (16)$$

$$E_{param}^T C E_{param} = 1, \quad (17)$$

where S is the scatter matrix $D^T D$.

The problem described is easily solved by eigen-vectors of Eq. (16). If (λ_i, u_i) solves (16), then it also does solve $(\lambda_i, \mu u_i)$ for any μ , and from (17) we can find μ_i that satisfies $\mu_i^2 u_i^T C u_i = 1$ by using

$$\mu_i \sqrt{\frac{1}{u_i^T C u_i}} = \sqrt{\frac{1}{u_i^T S u_i}}. \quad (18)$$

Finally, by applying $\hat{E}_{param_i} = \mu_i u_i$, we solve Eq. (18).

Thus, by the Fitzgibbon *et al.* (1999) scheme, the best parameters of the ellipse correspond to an eigen-vector identified by a minimal positive eigen-value.

5. Results

Eye fundus images were provided by the Department of Ophthalmology of the Institute for Biomedical Research of Kaunas University of Medicine (BRKU). The testing set consisted of 54 retinal images.

Within the scope of our investigation, only the retinal images of glaucomatous and healthy eyes were taken.

The results were evaluated by two criteria: optic nerve disc position in retinal image identification and approximation by ellipse accuracy.

In the first case, in the OD localization there was only one false result which leads the proposed algorithm to the accuracy of 98%. In the second case, in the optic nerve disc approximation by ellipse correctness measurements we excluded the case where the OD localization failed. Next, a comparative parameter space was constructed.

In this step, the ophthalmologists from the BRKU set the points describing the optic nerve disc boundary by hand in the provided retinal images. These fundus images were not scaled down. Further, the least squares method described above was incorporated to produce the parametric form of each optic disc from all the 54 retinal images. Since the reference points were set by ophthalmologists, the defined elliptic parameters formed a reference parameter space for the proposed automatic algorithm testing. As described in the least squares section, the rotation of ellipse is totally controlled by the algorithm. Besides, the reference points and that gathered by an automatic algorithm were provided to the same least squares algorithm to get a parametric cone representation.

The comparative parameter space was formed of major and minor axes as well as horizontal and vertical diameters of the ellipse. The vertical and horizontal diameters of a cone were used here to indirectly show and evaluate the rotation of the ellipse. For the approximated examples shown in Figs. 8, 9, 10 both data sets (ellipse parameters from the reference points and ellipse parameters from the proposed algorithm) is provided in Table 1.

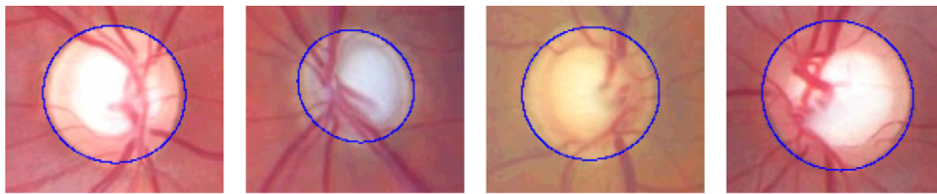


Fig. 8. Excellent approximation by the ellipse.

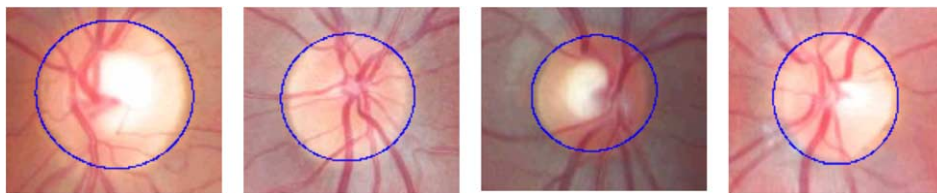


Fig. 9. Good approximation by the ellipse.

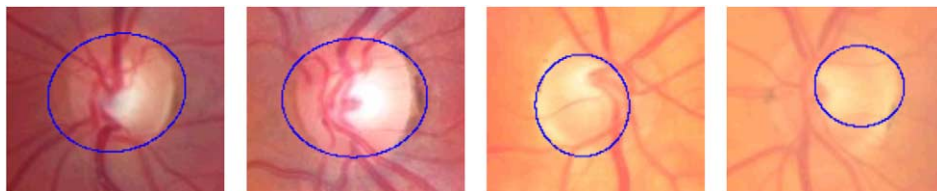


Fig. 10. Poor approximation by the ellipse.

Table 1
Some values from two data sets compared

Ellipse parameters from reference points				Ellipse parameters from proposed algorithm				Average error rate %
OD major axis	OD minor axis	OD horizontal diameter	OD vertical diameter	OD major axis	OD minor axis	OD horizontal diameter	OD vertical diameter	
2.54	2.44	2.44	2.54	2.56	2.46	2.54	2.49	1.89
2.18	2.09	2.09	2.18	2.17	2.08	2.14	2.08	1.96
2.27	2.15	2.19	2.22	2.28	2.16	2.19	2.19	0.52
2.28	2.16	2.18	2.25	2.22	2.11	2.11	2.21	2.44
2.22	2.06	2.08	2.20	2.29	2.07	2.23	2.12	3.54
2.43	2.29	2.31	2.41	2.45	2.43	2.42	2.42	3.02
2.59	2.56	2.53	2.51	2.49	2.42	2.47	2.40	4.02
2.30	1.97	1.98	2.19	2.34	1.95	2.19	1.98	5.80
2.45	2.43	2.42	2.42	2.50	2.29	2.21	2.21	6.19
2.41	2.02	2.04	2.39	2.40	2.21	2.40	2.21	8.64
2.22	2.15	2.20	2.18	1.70	1.57	1.57	1.73	24.81
2.25	2.14	2.21	2.18	1.51	1.35	1.50	1.34	35.22

The overall average error rate achieved for the major axis of the ellipse was 4.97%, for the minor axis – 6,06%, for the horizontal diameter – 9,26% and for the vertical diameter of the ellipse – 7,37%.

Such a high error rate of the horizontal and vertical diameters of the ellipse is self-explanatory. Since the OD in retinal images has nearly a circular shape (the average difference in the provided data-set of minor and major axes is 0,2mm), thereof the ellipse rotation angle with respect to the positive Cartesian of the axis x is very neat. In other words, OD has more degrees of freedom to be rotated to vouch for the best fit problem.

We assume that the excellent approximation is when the average of parameters from two sets differ less than 3%, a good approximation is when the average of parameters are between 3% and 6%, and a poor approximation is when the average of parameters is more than 6%.

As can be seen from Table 1, the last two lines the average error between parameters is more than 20%. In all such cases in eye fundus images the optic nerve disc has a very weak edge gradient and can hardly be seen even by eye, as shown in Fig. 10, the last two images. Consequently, the made up OD boundary data set collected is very small. This is because we restrict the radius r when selecting boundary points in the section of optic nerve disc approximation by the ellipse and that leads to the fact that the least squares method fails to produce the right parametric form of the ellipse.

Some examples of the algorithm work are provided in Figs. 8, 9, and 10.

6. Conclusions

This paper provides an efficient algorithm for the optic nerve disc localization and approximation by a parametric curve such as an ellipse. In the pre-processing step we have showed that after applying the morphological closing operation to decomposed image colour channels, the recombined result does not cause colour distortion in the retinal image, while the vascular tree is removed from the colour retinal image.

In the second section, the *Canny* edge detection algorithm was introduced to determine a boundary of the optic disc. The introduction of non-static threshold value computation by *Otsu's* method extended this algorithm. This extension automatically selects values for the *Canny* threshold depending on the intensity of each retinal image. To localize an approximate centre of the optic nerve disk, the iterative circular *Hough* transform was used that led the algorithm accuracy of the localization up to 98%.

Finally, the least squares method was applied to calculate the ellipse parameters on the set of OD boundary points. The resulting ellipse parameters were compared and showed that the elliptic parameters, obtained by the proposed algorithm, on the average did not differ from those obtained by the reference points more than 10%. Also, the reference points have been taken from a non-scaled down image, which shows that the loss of information is minor in this context of problem.

Acknowledgement

The research is partially supported by the Lithuanian State Science and Studies Foundation project "Information technology tools of clinical decision support and citizens wellness for e.Health system" No. B-07019.

References

- Ashbrook, A., and N.A. Thacker (1998). *Tutorial: Algorithms For 2-Dimensional Object Recognition*. Imaging Science and Biomedical Engineering Division, Medical School, University of Manchester, Manchester.
- Ballard, D.H. (1981). Generalizing the Hough transform to detect arbitrary shapes. *Pattern. Recognition.*, **13**, 111–121.
- Bookstein, F. (1979). Fitting conic sections to scattered data. *Computer Vision and Image Processing*, **9**, 56–71.
- Boyd, J. (1996). *STARE Software Documentation: Disk – Optic Disk Locator*. Technical report, Visual Computing Laboratory, Department of Electrical and Computer Engineering, University of California, San Diego.
- Canny, J. (1986). A computational approach to edge detection. *IEEE Trans. Pattern Anal. Mach. Intell.*, **8**, 679–698.
- Chaudhuri, S., S. Chatterjee, N. Katz, M. Nelson and M. Goldbaum (1989). Automatic detection of the optic nerve in retinal images. In *Proceedings of the IEEE International Conference on Image Processing*. pp. 1–5.
- Fitzgibbon, A.W., M. Pilu and R.B. Fisher (1999). Direct least-squares fitting of ellipses. *IEEE Transactions on Pattern Analysis and Machine Intelligence*, **21**(5), 476–480.
- Foracchia, M., E. Grisan and A. Ruggeri (2004). Detection of the optic disc in retinal images by means of a geometrical model of vessel structure. *IEEE Trans. on Medical Imaging*, **23**(10), 1189–1195.
- Goldbaum, M., S. Moezzi, A. Taylor, S. Chatterjee, J. Boyd, E. Hunter and R. Jain (1996). Automated diagnosis and image understanding with object extraction, object classification, and inferencing in retinal images. In *Proceedings of the IEEE International Conference on Image Processing*. pp. 695–698.

- Goutsias, J., H. Heijmans and K. Sivakumar (1995). Morphological operators for image sequences. *Computer Vision and Image Understanding*, **62**, 326–346.
- Grau, V., J.C. Downs and C.F. Burgoyne (2006). Segmentation of trabeculated structures using an anisotropic Markov random field: application to the study of the optic nerve head in glaucoma. *IEEE Transactions on Medical Imaging*, **25**(3), 245–255.
- Hoover, A., and M. Goldbaum (2003). Locating the optic nerve in a retinal image using the fuzzy convergence of the blood vessels. *IEEE Tran. on Medical Imaging*, **22**(8), 951–958.
- Hough, P.V.C. (1965). *A Method and Means for Recognizing Complex Patterns*. U.S. Patent 3069654.
- Lowell, J., A. Hunter, D. Steel, A. Basu, R. Ryder, E. Fletcher and L. Kennedy (2004). Optic nerve head segmentation. *IEEE Transactions on Medical Imaging*, **23**(2), 256–264.
- Mendels, F., C. Heneghan and J. Thiran (1999). Identification of the optic disc boundary in retinal images using active contours. In *Proceedings of the Irish Machine Vision and Image Processing Conference*. pp. 103–115.
- Morris, D.T., and C. Donnison (1999). Identifying the neuroretinal rim boundary using dynamic contours. *Image and Vision Computing*, **17**, 169–174.
- Otsu, N. (1979). A threshold selection method from gray-level histograms. *IEEE Trans. Syst. Man Cybernet.*, **SMC9**(1), 62–66.
- Peters, R. (1997). Mathematical morphology for angle-valued images. In *Non-linear Image Processing, International Conference on Electronic Imaging, Society of Photo-Optical Instrumentation Engineers*. pp. 1–11.
- Pinz, A., S. Bernogger, P. Datlinger and A. Kruger (1998). Mapping the human retina. *IEEE Trans. on Medical Imaging*, **17**(4), 606–619.
- Rao, S.S. (1984). *Optimization: Theory and Applications*. 2 edition. Wiley Eastern.
- Sinthanayothin, C., J.F. Boyce, H.L. Cook and T.H. Williamson (1999). Automated localization of the optic disc, fovea, and retinal blood vessels from digital colour fundus images. In *Br F Ophthalmol*. pp. 902–910.
- Soille, P. (1999). *Morphological Image Analysis*. Springer-Verlag, Berlin.
- Tian, H., S.K. Lam and T. Srikanthan (2003). Implementing Otsu's thresholding process using area-time efficient logarithmic approximation unit. *IEEE International Symposium on Circuits and Systems (ISCAS)*, vol. 4. Bangkok, Thailand. pp. 21–24.
- Tobin, K.W., E. Chaum, V.P. Govindasamy, T.P. Karnowski and O. Sezer (2006). Characterization of the optic disk in retinal imagery using a probabilistic approach. In *SPIE International Symposium on Medical Imaging. Proceedings*, vol. 6144. San Diego, California.
- Tolias, Y., and S. Panas (1998). A fuzzy vessel tracking algorithm for retinal images based on fuzzy clustering. *IEEE Trans. on Medical Imaging*, **17**(2), 263–273.
- Xu, J., O. Chutatape, E. Sung, C. Zheng and P.C.T. Kuan (2007). Optic disk feature extraction via modified deformable model technique for glaucoma analysis. *Pattern Recognition*, **40**(7), 2063–2076.

P. Treigys graduated from the Vilnius Gediminas Technical University, Lithuania. Since 2005 is a doctoral student of the System Analysis Department of the Institute of Mathematics and Informatics, a lecturer at the Vilnius College of Higher Education. He is a member of Lithuanian Society for Biomedical Engineering. His interests include: image analysis, detection and object's feature extraction in image processing, automated image objects segmentation, optimization methods, software engineering, artificial neural networks.

V. Šaltenis graduated from the Kaunas Technological Institute, Lithuania. He received a PhD degree from the Moscow Energy Institute of the USSR Academy of Sciences in 1966 and the degree of habil. doctor from the Institute of Mathematics and Informatics, Vilnius in 1998. He was a principal researcher of the Optimization Department at the Institute of Mathematics and Informatics, Lithuania. His research interests included both theory and applications of the structure of optimization problems, data and image analysis.

G. Dzemyda graduated from Kaunas University of Technology, Lithuania, in 1980, and in 1984 received there the doctoral degree in technical sciences (PhD) after post-graduate studies at the Institute of Mathematics and Informatics, Vilnius, Lithuania. In 1997 he received the degree of doctor habilius from Kaunas University of Technology. He was conferred the title of professor (1998) at Kaunas University of Technology. He is a director of the Institute of Mathematics and Informatics and heads the System Analysis Department of the institute. The areas of research are the theory, development and application of optimization, and the interaction of optimization and data analysis. The interests include optimization theory and applications, data mining in databases, multiple criteria decision support, neural networks, parallel optimization, internet databases, the models of epidemic spread.

V. Barzdžiukas graduated from the Kaunas University of Medicine, Lithuania. 1988 Candidate of medical sciences in Odessa V. Filatov Eye Disease and Tissue Therapy Research institute. 1994 notification of doctor of medicine degree (Ph.D.), since 1999 associate professor. Member of telemedicine project group of Kaunas University of Medicine since 1999, participant of Lithuanian–Swedish telemedicine projects Litmed; Baltic Medweb; Baltic Medweb II. His research interests include non-invasive investigations of haemodynamic in ophthalmology, teleophthalmology.

A. Paunksnis graduated from the Kaunas University of Medicine, Lithuania. Medical doctor since June, 1969. Dr. Sci (habil.) since 1993. Professor of ophthalmology since 1997. He is director of Department of Ophthalmology, Institute for Biomedical Research of Kaunas University of Medicine since July, 1992. Member of Council of European Ophthalmologist Society since 1995. Full member of International Society of Experimental Eye Research since 1989, President of Lithuanian Ophthalmologist Society 1993 to 1997. Chairman of Council of Kaunas University of Medicine 1997 to 2000. Coordinator of Telemedicine project group of Kaunas University of Medicine since June 1999. Head of Telemedicine Center of Kaunas University of Medicine since 2002. His present research areas include non-invasive ultrasound examination in ophthalmology, ophthalmocology, epidemiology, telemedicine.

Automatinis akies nervo disko parametrizavimas

Povilas TREIGYS, Vydūnas ŠALTENIS, Gintautas DZEMYDA,
Valerijus BARZDŽIUKAS, Alvydas PAUNKSNIS

Akies dugno tyrimas yra viena iš svarbiausių oftalmologijos diagnozavimo procedūrų. Akies dugno nuotrauką sudaro trys grupės struktūrų: akies nervo diskas, kraujagyslės ir tinklainė. Atskiru atveju akies nervo diske gali būti stebima pakitusi ekskavacija. Taigi, automatinis akies dugno nuotraukoje esančių struktūrų klasifikavimas ir parametrizavimas galimas tik aiškiuose (kokybiškuose, aiškiai išreikštos anatomicinės struktūros) vaizduose. Tokio tipo nuotraukų kompiuterizuota automatinė analizė yra ypač sudėtinga. Be to, automatinis optinio nervo disko lokalizavimas ir parametrizavimas yra svarbi oftalmologinė procedūra nustatant glaukomos diagnozę, kadangi pagrindiniai ligą nusakantys požymiai yra parametru santykiai tarp akies nervo disko bei galimai pakitusios ekskavacijos. Šiame straipsnyje autoriai pateikia algoritmą automatiniam akies nervo disko lokalizavimui bei parametrizavimui elipse spalvotose akies dugno nuotraukose. Taip pat, straipsnyje yra aptariami siūlomo algoritmo darbo rezultatai.